Solid Freeform Fabrication 2019: Proceedings of the 30th Annual International Solid Freeform Fabrication Symposium – An Additive Manufacturing Conference
Reviewed Paper

Moisture Effects on Selective Laser Flash Sintering of Yttria-Stabilized Zirconia

Deborah Hagen[1], Alex Chen[1] Joseph J. Beaman[1], and Desiderio Kovar,[1,2]
[1]Department of Mechanical Engineering

[2]Materials Science and Engineering Program
University of Texas at Austin
Austin, TX 78712

Abstract

Selective laser flash sintering (SLFS) combines a uniform electric field with a localized, scanning laser as the only external heating source. The presence of a large uniform electric field can greatly increase the sintering rate and lower the sintering temperature for ceramics. The combination of lower sintering temperature and faster sintering rates may allow SLFS to be used for ceramic additive manufacturing. In this work, we study the effects of moisture on SLFS of yttria-stabilized zirconia ceramic. We compare the effects of processing parameters on the initiation of SLFS for samples exposed to a range of moisture levels.

Introduction

Ceramics are challenging to process because they cannot be easily melted due to their very high melting points. Thus, standard methods for processing ceramics require furnace-based heating that enables slow diffusion of atoms in the solid state over a period of hours until porosity is eliminated. To adapt these processes to additive manufacturing, shape formation is accomplished by temporarily fusing the powder particles together with polymers.[1, 2] After shape formation, subsequent slow pyrolysis is used to convert the polymers into gaseous by-products that must escape through open porosity in the ceramic body. That porosity is then reduced or eliminated, and the ceramic powders are fused to one another during a higher temperature furnace firing of the ceramic. This process can be used for part geometries that have at least one small dimension because the pyrolysis becomes extremely challenging for large, solid parts.[3, 4]

An alternative is to directly sinter ceramic powder particles together rather than using polymers to define the shape. However, this has proven challenging to achieve in practice because diffusional processes required for conventional sintering are generally too slow at reasonable laser fluences. At higher fluences, cracking due to thermal shock is a challenge.[5]

Within the last decade, it has been established that sintering rates can be dramatically accelerated by combining a high electric field to a ceramic being heated in a furnace environment.[6] The furnace-based flash sintering process dramatically increases sintering rates by orders of magnitude, leading to a complete sintering of many types of ceramic in a few seconds rather than hours.[7] In most studies of furnace-based flash sintering, a DC electric field is applied to the ceramic body using electrodes attached to the sample. Ceramics are generally large

bandgap semiconductors and thus their electrical conductivity increases with temperature. As they are heated and conductivity increases, current begins to flow if a strong enough electric field is applied. Thus, additional heating occurs due to Joule heating.[8, 9]

Flash sintering has three stages, classified based on the magnitude of the current flow and its rate of increase, and on the densification of the ceramic powder compact.[10] In stage I, the onset of electrical current flow becomes measurable and starts to increase. During this stage, necks between ceramic particles begin to form. There is typically minimal densification of the ceramic body during stage I flash sintering. In stage II, there is a rapid increase in current, which can run away if not halted. Densification of the ceramic body proceeds rapidly. In most studies of flash sintering, the power supply controlling current flow is switched from voltage to current control mode when a critical current is reached, and current is limited to a moderate flow. This constant current regime defines stage III where any remaining porosity is further reduced or eliminated.

Selective laser flash sintering (SLFS) uses a scanning laser as the only external heating source in combination with a high electric field. The SFLS technique can increase the sintering rates to potentially enable this process to be used for additive manufacturing of ceramics. Preliminary SLFS experiments showed that there was significant day-to-day and sample-to-sample variability in the processing conditions required to initiate SLFS. Since a robust and repeatable process is critical to any manufacturing process, it is important to understand and reduce any sources of variability. Although there have been no previous studies of the effects of moisture on SLFS, recent studies have shown that moisture adsorbed on ceramic powders can alter the conditions required to initiate furnace-based field-assisted sintering. For example, Dargatz *et al.* studied the effect of adsorbed water during spark plasma sintering and showed that ZnO with adsorbed water fully densified at temperatures that were 400˚C lower than those required for a dry ceramic.[11] Nie *et al.* showed moisture reduced the temperature required to flash sinter ZnO to room temperature.[12] In our SLFS system, powders are at room temperature until lasing begins, and the presence of moisture therefore has the potential for affecting the SLFS process.[13, 14]

This study reports on the effects of adsorbed moisture in the SLFS process. We compare ceramic powder compacts that were in equilibrium with laboratory air and samples that were dried prior to SLFS. The focus is on the stage I SLFS, where current begins to flow without densification, and stage II SLFS where current rises steeply and densification is rapid.

Experimental Procedures

The ceramic powder was an 8 mol% yttria-stabilized zirconia (Tosoh TZ-8Y, Japan). Pellets were used rather than a loose powder bed to facilitate handling for sample analysis and to allow quantification of the moisture content. The powder was pressed as-received into a short cylindrical pellet with a 25.4 mm diameter and 2.5 - 3 mm thickness using a carbide die with steel plungers. The die set was lightly lubricated with a steric acid/acetone solution prior to the pressing to prevent the powder from sticking to the die or plungers. The acetone was evaporated at room temperature from the solution after coating the die set and prior to putting the powder into the die set. The die set containing powder was inserted into a manual press and uniaxially

pressed at 35 MPa. The pellet was removed from the die and the surfaces were gently wiped several times to remove any residual steric acid from the surface.

Electrodes were painted onto one surface of the pressed pellet using colloidal silver suspended in isopropanol (PELCO, Ted Pella, Redding, CA). A diagram of the pellet with painted electrodes is shown in Figure 1. The parallel vertical lines are the regions that were scanned with a laser. The central laser scan lines bridge the positive and negative electrodes. The short laser scan lines on the far right and left sides are fiducial marks. The arrow shows the direction of the laser scan. The laser scan proceeds so that it begins on the positive electrode and proceeds until the laser is on the negative electrodes at the end of the line scan.

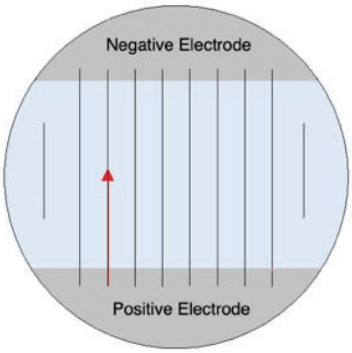

Figure 1: A plan view schematic of the ceramic pellet shows the location of electrodes and laser scan lines.

A custom-built selective laser flash sintering (SLFS) system was used for the experiments that is schematically illustrated in Figure 2. Energy was applied to the sample with a continuous-wave, infrared CO_2 laser with a 10.6 µm wavelength (Model 48-5, Synrad, Mukilteo, WA). The beam was focused at the surface of the ceramic sample using ZnSe-coated optics (Edmund Optics, Barrington, NJ). The width of the scans was 25 mm or less, and the distance from the scanning mirrors to the sample was 30 cm. The theta angle with this geometry is minimal, so optics compensation for beam shape and focus was not used. The beam at the specimen surface had a Gaussian profile with a full width at half of maximum (FWHM) diameter of 365 µm, as measured using a beam profiler (NanoScan v2™, Ophir, Jerusalem, Israel). The laser was rastered across the sample surface using a pair of ZnSe mirrors connected to high-speed galvanometers (6240H, Cambridge Technology, Bedford, MA).

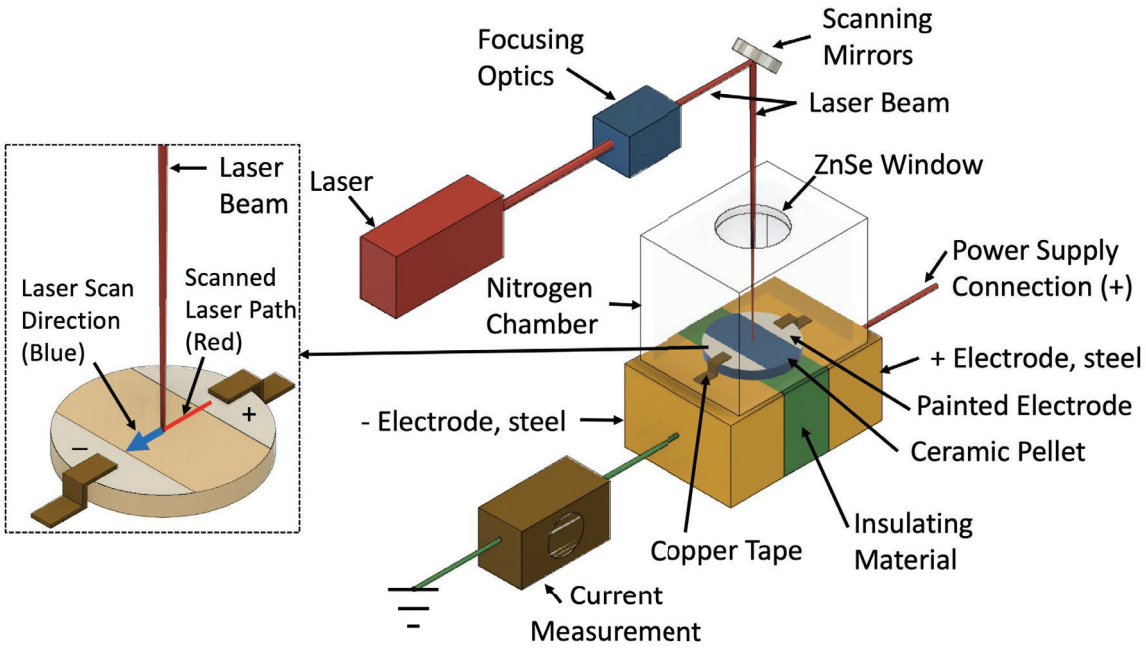

Figure 2: Overview schematic of SLFS machine

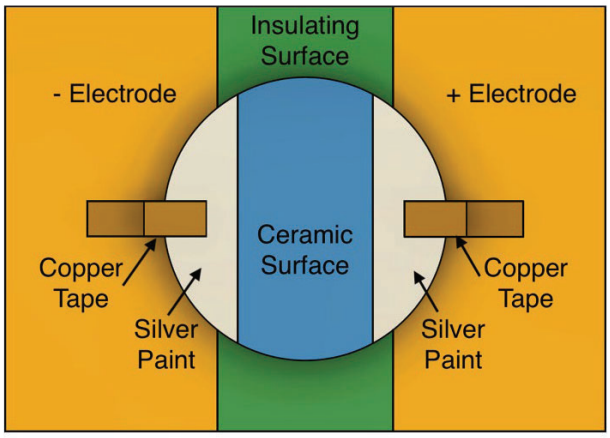

Figure 3: Schematic of the portion of the SLFS machine containing the build platform and electrodes

The ceramic pellet was placed on the build platform between the two electrodes. The painted electrodes on the pellet were taped to the corresponding electrodes in the SLFS system with copper adhesive tape to provide an electrical path from the DC power supply (PS350, Stanford Research Systems, Inc., Sunnyvale, CA) to the surface of the ceramic pellet. An acrylic fixture was used to center the pellet under the laser target area, as shown in Figures 3 and 4. The sample was placed within a custom-made acrylic chamber that enclosed the build platform. The chamber contained a ZnSe window so that the laser beam could be rastered on the sample surface. The samples were placed in the chamber, and the chamber was backfilled with nitrogen beginning approximately two minutes before scanning. A 6.9 kPa positive pressure of nitrogen was then maintained throughout the experiment. The electric field was turned on approximately one minute prior to scanning.

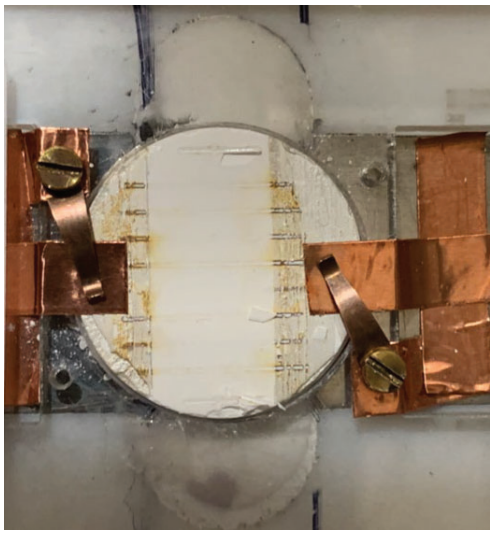

Figure 4: Plan view of a pellet on the build platform surface, with transparent acrylic fixture for aligning the pellet. Stainless steel electrodes are located on the build surface at top and bottom of photo. Copper tape and copper clips connect the silver painted electrodes to the stainless-steel electrodes. Photo was taken after the part was lased.

The laser was the only heating source, and the samples were at room temperature prior to scanning. To limit the number of potential variables, the only processing parameters that were varied from scan line to scan line were the laser power and electric field strength. The laser power ranged from 8 W to 20 W and the field strength was varied from 0 - 3000 V/cm. For these experiments, only a single layer was laser-scanned. The order in which the lines were scanned was randomized on each pellet and a total of 14 pellets were examined for this study.

The scan pattern on each pellet consisted of eight or nine parallel single line laser scans, depending on the pellet, as shown in Figure 1. The scan lines were oriented perpendicular to the edges of the electrodes and started on the positive electrode and travelled onto the negative electrode. The laser beam raster speed was fixed at 100 mm/s, and the pitch between the scan lines was 2.3 or 2.15 mm. This pitch was large enough to eliminate direct laser interaction between the lines. A wait time of approximately 1 minute was used between scanning of neighboring parallel lines to decrease thermal effects from previous scans. An infrared (IR) camera (SC8200 FLIR, Wilsonville, OR) was used to verify that the ceramic surface cooled below the 150˚C minimum detection range of the camera. Two shorter scan lines were located at the left and the right of the pellet that did not form a complete path between electrodes. These lines were produced by scanning at a higher energy density (50 mm/s, 7.7 W) and functioned only as fiducial marks. The laser scan lines on the specimen surface are not visible with optical microscopy for many of the laser parameters tested. Because the fiducials were scanned with high fluence, they allowed the determination of the locations of the other laser scan lines.

Electrical current through the sample was measured using a data acquisition and control system (Compact RIO 9035, National Instruments, Austin, TX) with a current measurement

module (NI-9207, National Instruments, Austin, TX). The current measurements were recorded between the negative electrode and ground. The laser signal was monitored with a voltage measurement module (NI-9201, National Instruments, Austin TX). Current and voltage measurements were recorded every 2 ms with a precision of +/-0.87%. The laser voltage signal was recorded simultaneously with specimen current to correlate current with the laser on/off times. The current on the power supply was limited to 2.5 mA. The DC power supply was automatically interrupted when the predetermined current limit was reached. Custom LabView and MATLAB software was used to record and analyze the data.

The FLIR infrared camera was used in an attempt to measure the surface temperature during SLFS. The camera was equipped with a 50 mm lens with an ND2 filter attachment is used to record data through a ZnSe window on the acrylic nitrogen chamber. The ND2 filter was required for the camera to image higher temperatures. The camera had a field of view of 256×256 pixels and data were recorded at a wavelength of 3-5 μm and a frequency of 474.1 Hz. The spot size on the sample was approximately 150×150 μm. The emissivity of 8% yttria-stabilized zirconia is nonlinear over the wavelengths of 3-5 μm, so a material-specific calibration curve was used to convert the raw count data into nominal temperature.[15]

In this evaluation, dry pellets were compared with pellets in equilibrium with laboratory air. Pellets were dried in an oven for at least 2 hours at 125˚C and then immediately moved into the SLFS chamber where they were exposed to a dry nitrogen atmosphere. The dried pellets were compared to samples that were in equilibrium with laboratory air. For this condition, pellets were left on the laboratory bench for at least 2 hours before placing them into the SLFS system with dry nitrogen atmosphere. The first laser scan started within 1 minute and all scans were completed within 15 minutes after placing the samples into the SLFS system.

The moisture adsorption rate in laboratory air was measured by removing a pellet without electrodes from the oven and immediately placing it onto a precision balance in laboratory air. Mass was recorded until no observable change occurred. To confirm that the pellets were in equilibrium with the laboratory air, the pellet was then left for 16 hours in the laboratory air; in each case, the pellet mass did not increase further. For the determination of maximum pellet moisture adsorption, the pellet was placed inside a sealed glass desiccator containing de-ionized water. The pellet was stored in this 100% humidity chamber for 48 hours, and then the pellet was removed from the humidity chamber and the mass was measured. The pellet was then baked in an oven for 2 hours at 125˚C, and the mass was measured.

After the lines on the pellet were laser-scanned, the pellets were removed from the SLFS machine, and the scanned surfaces were gold-coated to allow the microstructures to be examined in a SEM (Vega 3, Tescan-Orsay, Czech Republic).

Results

Figure 5 shows the mass gain as a function of time for a dry pellet exposed to laboratory air. The pellet adsorbs moisture relatively quickly in laboratory air, reaching equilibrium within 30 minutes of removal from a dry environment. The mass gain for three pellets measured on the same day were 0.47%, 0.50%, and 0.48%. Mass gain measurements on two different days resulted in a 0.37 % increase in mass on one day, and in 0.49% mass increase on another day.

Figure 6 shows the increase in mass for three pellets exposed to laboratory air and three pellets exposed to the 100% humidity chamber. The increase in mass for pellets exposed to a 100% humidity environment is substantially higher, averaging 3.3% for the three pellets.

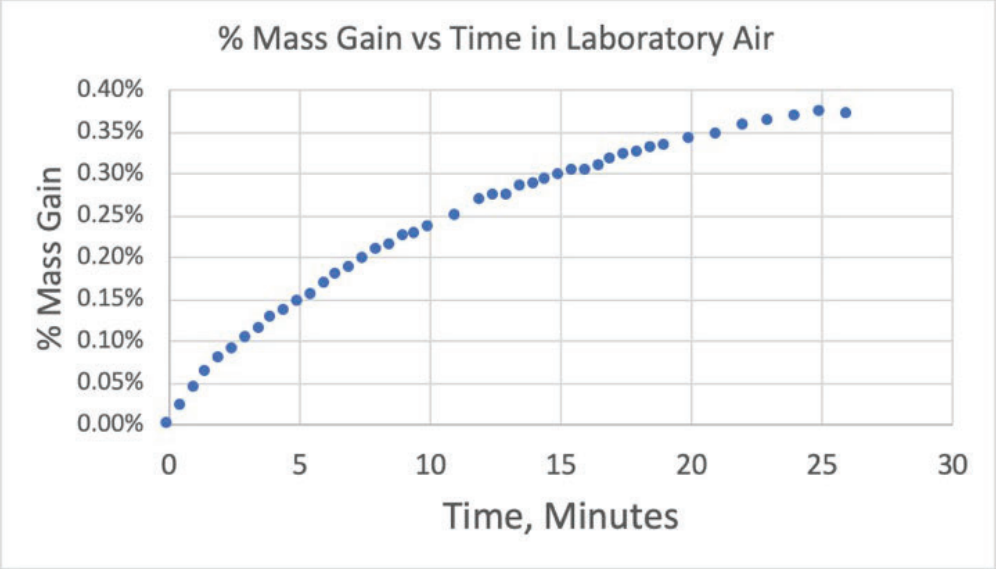

Figure 5: Mass increase versus time for a dry ceramic pressed pellet exposed to laboratory air.

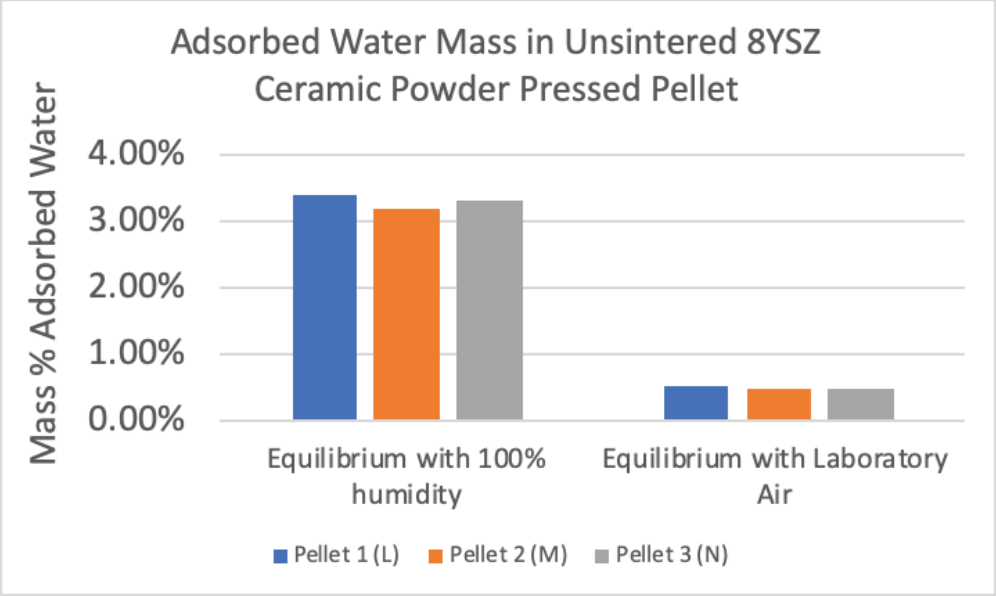

Figure 6: Comparison of water adsorption mass for three samples in equilibrium with a 100% humidity environment and for three samples that were in equilibrium with laboratory air.

To assess leakage current for samples that were exposed to electric fields, the field was first applied to the samples at room temperature without lasing. Figure 7 shows the effect of moisture on leakage current. Pellets that adsorbed moisture from laboratory air conduct electrical current at room temperature. In contrast, the dry pellets do not have a measurable

leakage current at room temperature. For the samples exposed to laboratory air, the leakage decreases over time in the dry nitrogen environment while under the electric field.

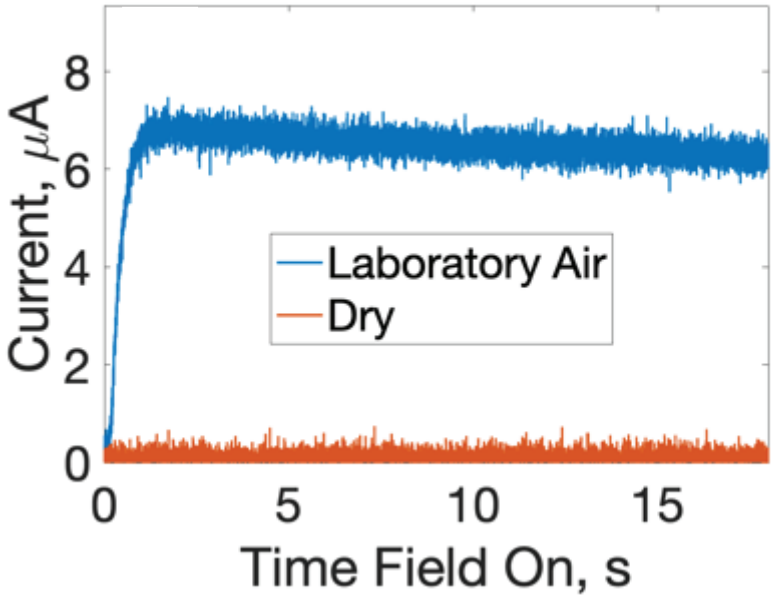

Figure 7: Comparison of leakage current for dry pellet and pellet in equilibrium with laboratory air. Power supply was turned on at time 0 on the graph. Field strength was 2000 V/cm.

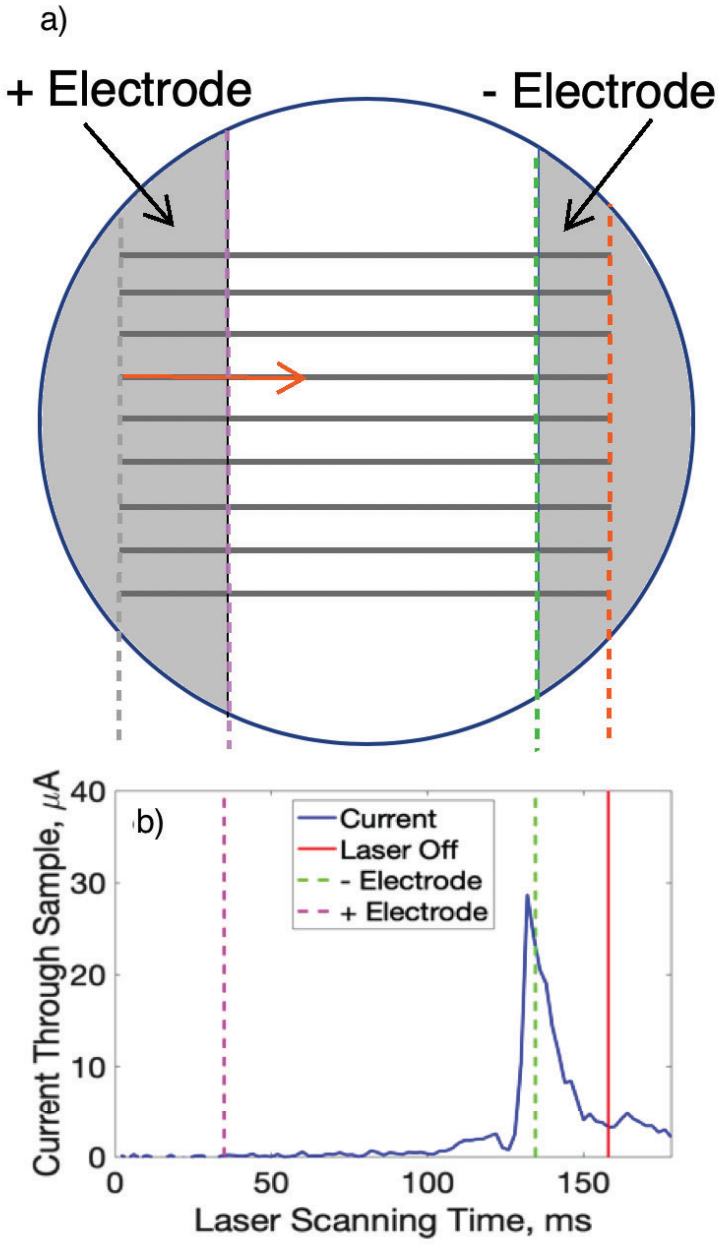

Figure 8: Correlation between laser beam position on the surface of ceramic pellet and current measured through the sample.

Electrical current data was measured during the laser scans to detect the onset of flash sintering. Figure 8 shows the correlation between the scan path of a laser line (Figure 8a) and the current measurement plot (Figure 8b). The left axis of the current plot (Fig 8b), at time = 0, corresponds to the point at the far left of a scan line in Figure 8a, when the laser turns on and begins to move to the right. The pink dotted line in both Fig. 8a and Fig. 8b represents the time when the laser moves beyond the silver painted electrode onto bare ceramic. The green dotted

line represents the time at which the laser reaches the negative electrode, and the solid red/orange line represents the point at which the scan line is completed, and the laser turns off. The graph (Figure 8b) extends an additional 20 ms beyond the time the laser is turned off in order to record the decay of current.

Figure 9 shows the apparent temperature as the laser scans over the sample. A path of higher temperature/least resistance is created for the current to travel from the positive to negative electrodes. When the laser reaches the negative electrode, a defined hot path is created and the current spikes dramatically, which can be seen in Figure 8b at around 130 ms. This behavior occurs when the laser power, laser scan speed, and applied electric field are sufficient to initiate SLFS.

Although it may be possible to measure relative differences in temperature using this IR camera, care should be taken in quantitatively interpreting these plots. Accurate temperature measurement of the SLFS process is extremely difficult given the small region of interest where the temperature is high, the speed of the process, and temperature-dependent emissivity of the material. The IR camera may not capture peak temperatures because temperature gradients are large, and the field of view is relatively large compared to the region of interest. This means the measured temperature with a pixel is the spatially averaged temperature within this pixel rather than the peak temperature. The flash occurs relatively quickly, as seen by the rapid current rise that occurs in milliseconds; this is much faster than the capture rate of the IR camera. Thus, the measured temperature is also a time average that includes both the peak temperature as well as cooling. The nonlinear emissivity of the pellet in the 3-5 μm detection wavelength range is also a challenge, since the porous surface and rapidly changing temperature can both affect the final temperature reading. Additionally, water vapor in the pellets or above the pellets due to heating can absorb IR radiation, decreasing the apparent magnitude of the temperature reading. In summary, it is likely that these measurements are underestimates to the actual temperatures. We are current exploring other methods for more accurately measuring temperatures at time and spatial scales appropriate for SLFS.

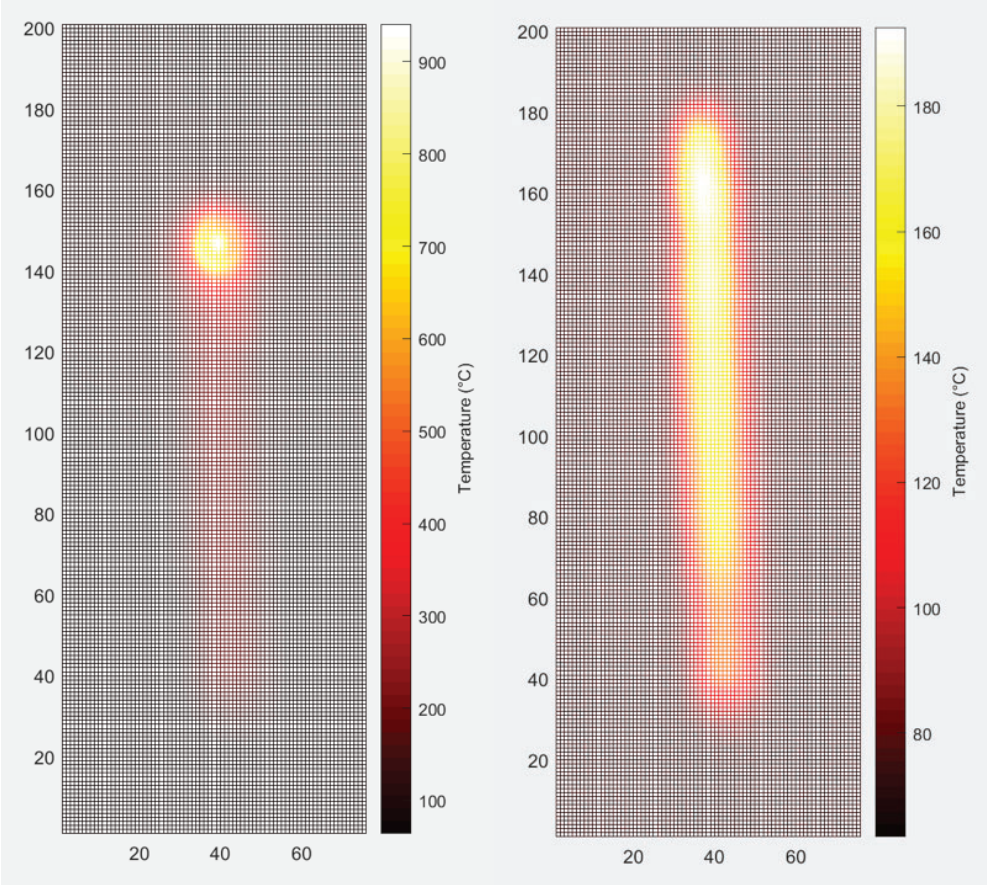

Figure 9: Apparent temperature recorded from IR camera intensity maps. The map on the left shows when the maximum temperature is recorded during laser scan. The map on the right shows the temperature profile shortly after laser beam is turned off.

Representative plots of different regimes in behavior are shown in Fig. 10. Figure 10a shows a sample with no observable room-temperature conductivity and scanning conditions that were insufficient to initiate SLFS. In this case, baseline noise (± 0.5 μA) is centered at zero current and there is no discernable rise in current as the laser beam heats that path between electrodes. Figure 10b shows leakage current, indicating that the sample is conductive and characterized by a baseline current that is not centered on zero. Again, the scanning conditions are such that SLFS is not initiated and there is no discernable rise above baseline as the laser nears the second electrode. Figure 10c and Figure 10d show a small to moderate spike in current as the laser approaches the negative electrode, indicating that stage I SFLS was initiated. The sample in Fig. 10c exhibits a measurable leakage current prior to beginning the scan whereas the sample shown in Fig. 10d does not exhibit a measurable leakage current. Figure 10e and Figure 10f show plots for samples where scanning conditions resulted in the initiation of stage II SLFS. In this case a much larger spike in electrical current is apparent compared to Figs. 10c and 10d, which triggers the current limit of the DC power supply.

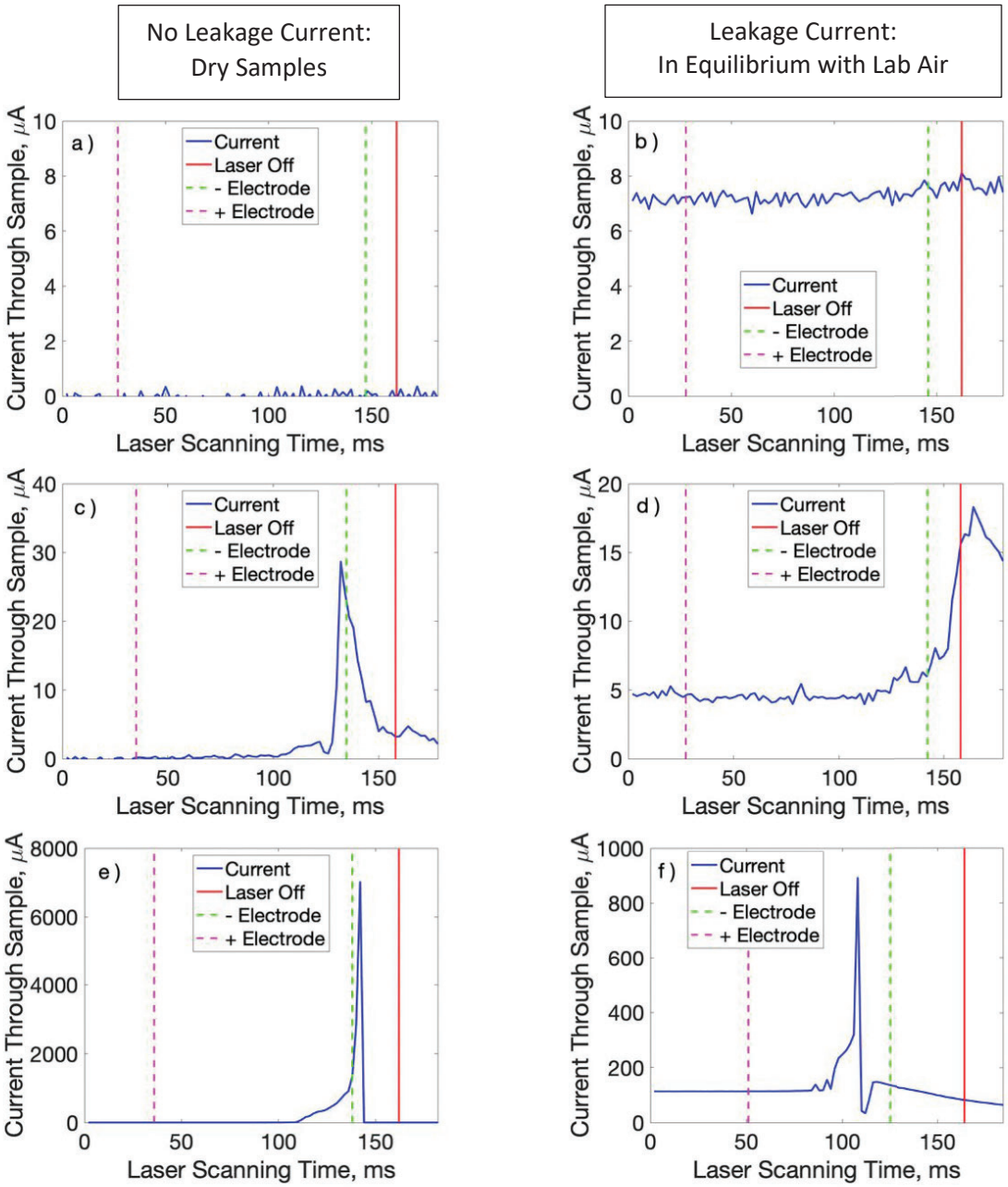

Figure 10: Categories of current behavior in SLFS line scans. a) Random noise without leakage, b) random noise with leakage current, c) moderate to low current rise without leakage current, d) moderate to low current rise with leakage current, e) large current rise without leakage current f) large current rise with leakage current

The effects of adsorbed moisture on the initiation of SLFS are shown in Fig. 11 for samples scanned at laser powers of 10-12 W. For dry samples scanned at 2000 V/cm, about 65% of the samples did not initiate SLFS and about 35% of these samples did initiate stage I SLFS. In contrast, all of the samples that were at equilibrium with laboratory air and were scanned at a field of 2000 V/cm exhibited stage I SFLS. At a higher field strength of 3000 V/cm, all of the samples that were exposed to moisture exhibited either stage I (65% of the samples) or stage II SLFS (35% of the samples). For the dry samples scanned at a field strength of 3000 V/cm, there

was more variability in the responses; almost 20% of the samples did not initiate SLFS but more than 20% of the samples exhibited stage II SFLS. Electrical conductivity increases sharply with temperature in this material. Slight changes in local packing density and local temperatures along the scan line would result in electrical conductivity changes. These are likely causes of the variation in the current through the samples, but additional work is necessary to quantify.

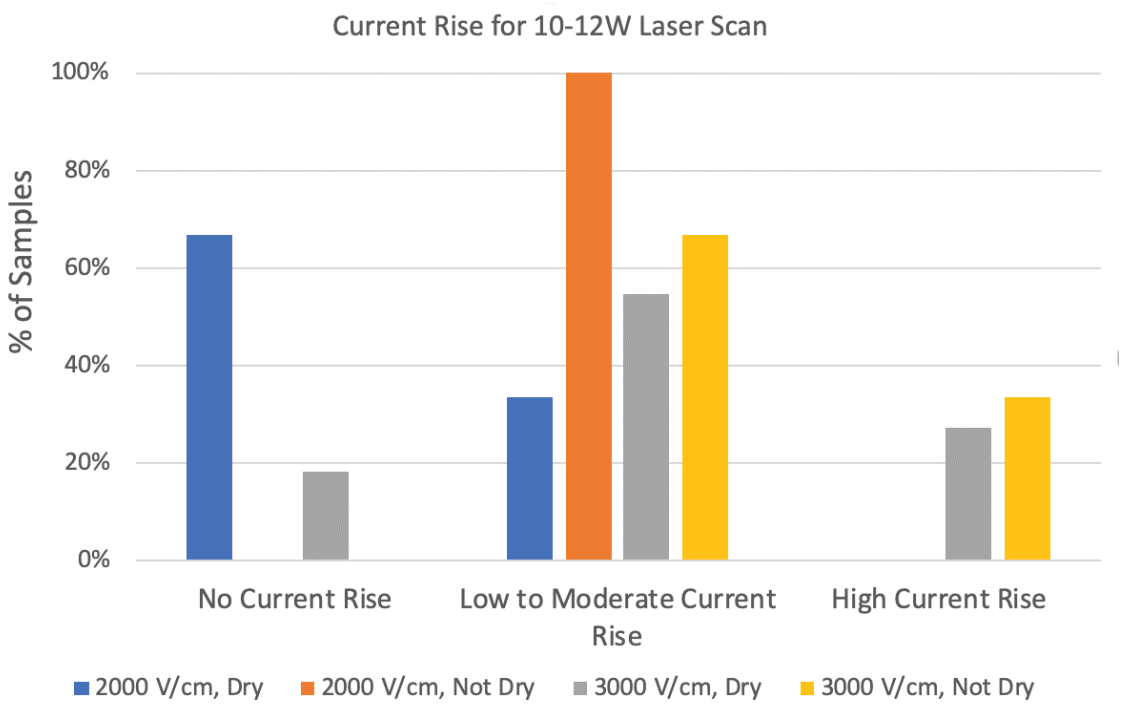

Figure 11: Percentage of samples exhibiting a measurable current rise for dry samples and samples exposed to moisture. Samples were scanned at a laser power of 10-12 W and field strengths of 2000 V/cm - 3000 V/cm.

To further explore the effects of laser power on the initiation of SLFS, additional experiments (not shown) were conducted for laser powers of 8 W. All of the samples exposed to laboratory air were observed to initiate stage I SLFS. In contrast, none of the dry samples that were scanned at 8 W exhibited SLFS. The dry samples did not exhibit a leakage and there was no current rise, similar to the current graph in Figure 10a. This is consistent with the hypothesis that moisture in the samples facilitates SLFS.

Microstructures of pellets that were scanned at 10 - 12 W for dry pellets and pellets exposed to laboratory air are shown in Figure 12. Samples that exhibited no current or moderate current do not exhibit significant consolidation or neck formation that is visible in SEM imaging. The neck development between particles seems more well-developed in the sample exposed to lab air that in the dry specimen. In contrast to samples with moderate current, samples that were scanned under conditions that resulted in a large current rise appeared to be partially melted.

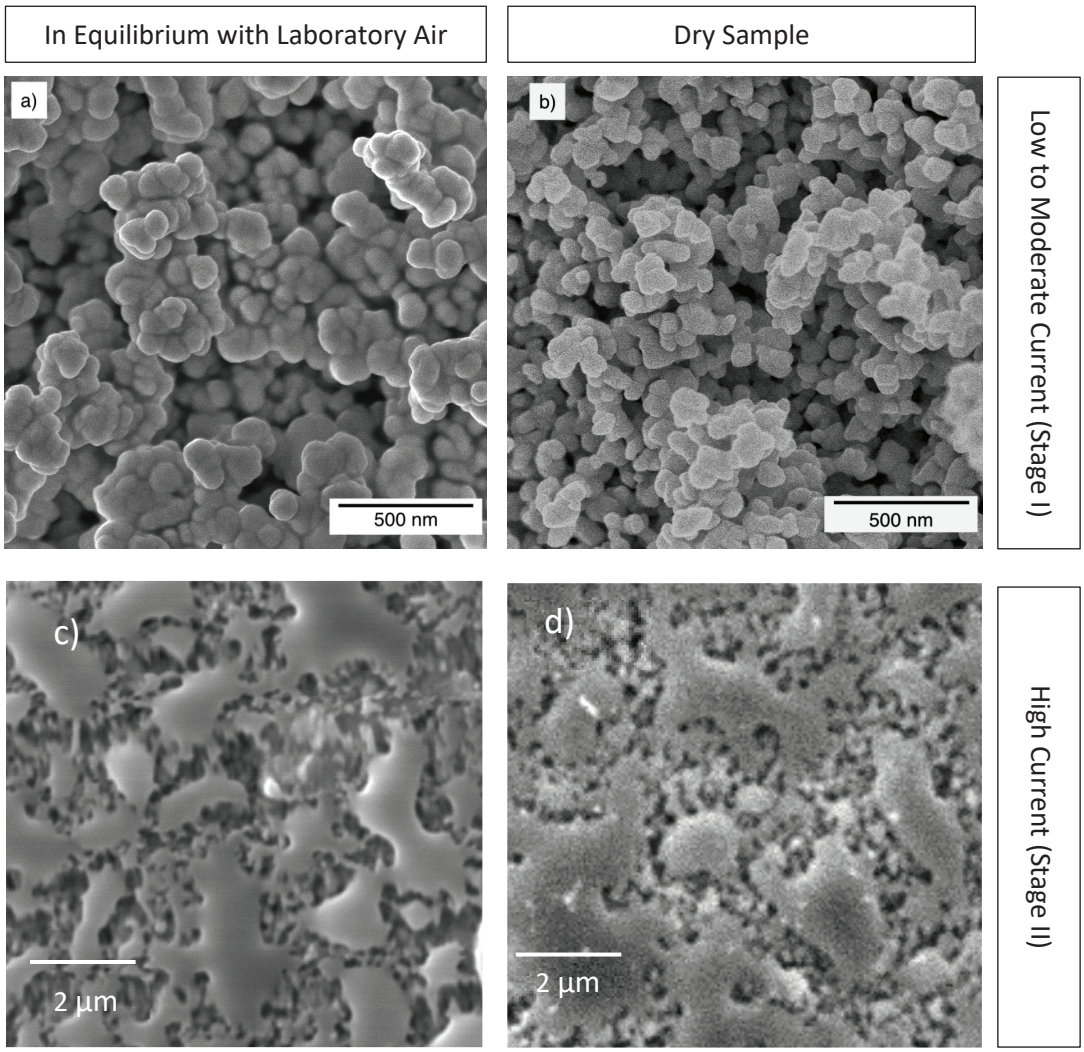

Figure 12: Microstructures for samples scanned at laser powers of 10-12 W: a) low to moderate currents for pellet exposed to laboratory air (10W laser power), b) low to moderate currents for dry pellet (10W laser power), c) high current for pellet exposed to laboratory air, d) high current for dry pellet

Increasing laser power from 10 W - 12 W to 15 W - 20 W didn't increase current flow in either dry samples or samples exposed to laboratory air. In fact, the current decreased in all cases compared to the samples scanned at 10 - 12 W. The samples scanned at laser powers of 15 W - 20 W laser powers cracked severely, and the resulting cracks likely affected the conductivity of the samples. SEM observations of the microstructures, shown in Figure 13, revealed that neck growth and consolidation of the particles occurred for both dry pellets and those exposed to laboratory air.

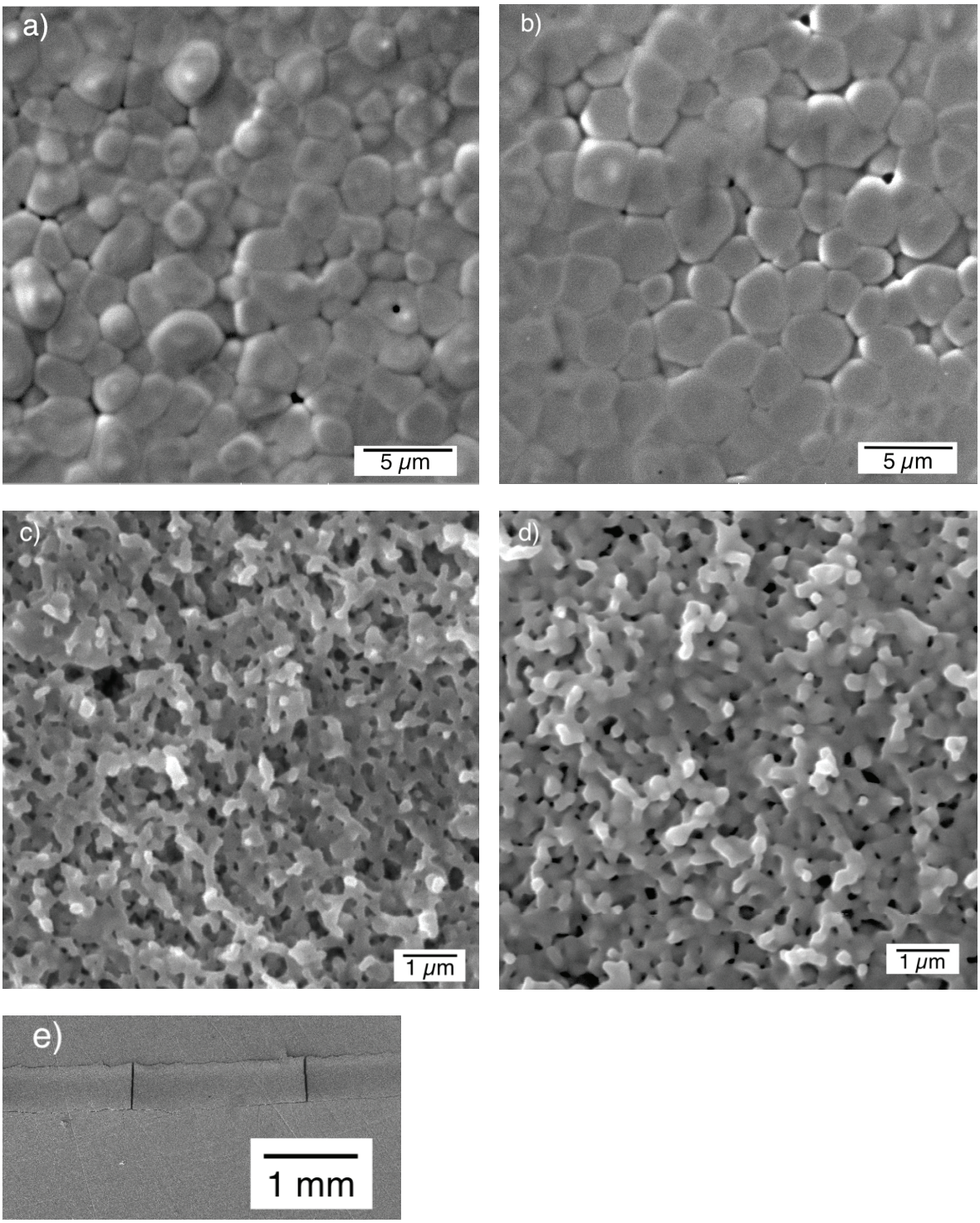

Figure 13: Microstructures of lines lased at 20 W laser power. a) pellet exposed to laboratory air, 3000 V/cm field strength. b) dry pellet, 3000 V/cm field strength. c) pellet exposed to laboratory air, no applied field. d) dry pellet, no applied field. e) Low magnification SEM shows cracked surface of a sample scanned at 20 W laser power.

Figure 13 shows the microstructural effects of pellet moisture and applied field in after lasing at 20 W laser power and 100 mm/s scan speed. Samples shown in Figure 13a and Figure 13b were scanned with no electric field. Samples shown in Figure 13c and Figure 13d were scanned with an applied electric field of 3000 V/cm. The samples on the left (Figures 13a and 13c) were exposed to laboratory air. The samples on the right (Figures 13b and 13d) were dry. Powder consolidation is evident in all of the samples, although the degree of densification is greater and grain growth is evident for the samples that were scanned with an applied field.

Discussion

The ceramic powder used in this study, 8% yttria-stabilized zirconia, was shown to readily adsorb moisture from the atmosphere when exposed to laboratory air. Weight gain measurements demonstrated that compacted pellets with a thickness of 3 mm - 3.5 mm reached equilibrium with moisture in the laboratory air within 30 minutes at room temperature (Fig. 5). Samples exposed to laboratory air absorbed less moisture than those exposed to a 100% relative humidity environment (Fig. 6). It is notable that the weight increase for samples exposed to laboratory air varied significantly from day to day. This confirms that adsorbed moisture in ceramic pellets is sensitive to the storage environment.

Moisture adsorbed in the pellet was shown to dramatically increase the sample conductivity when an electric field was applied to the sample (Fig. 7). For pellets that were in equilibrium with laboratory air, leakage currents of about 100 μ A were measured at fields of 2000- 3000 V/cm. When the samples were exposed to 100% humidity prior to testing, the leakage current was much higher. In fact, it was so high that it exceeded the maximum current typically used for SLFS. These results confirm that moisture strongly effects the conductivity of the pellets.

It was observed that the leakage current decreased over the time that the pellets were in the dry nitrogen environment under an applied field. It is likely that this decrease occurred due to sample drying while in the SLFS system. There are two contributing factors that can result in drying: 1) The dry nitrogen used in the chamber increases evaporation rates of water, even at room temperature and 2) Joule heating due to the leakage current. If the current is flowing primarily through an adsorbed water layer, the resistance of the current path through the water raises the temperature of the water and the powder particle surface. Over time, the increased temperature will in turn cause evaporation of the water, decreasing the thickness of the adsorbed water layer, and therefore increasing the resistivity of the pellet.

The decrease of moisture over time in the SLFS system appears to be inevitable unless the atmosphere of the SLFS system is purposely humidified to retain the water. This is possible, but is it desirable? In order to answer that question, it is necessary to determine what effect the moisture and associated leakage current has on the SLFS process. This is particularly important for stage I flash sintering, because this is the stage in which the particles begin to fuse together to define a solid shape distinct from the surrounding loose powder.

Current measurements taken during scanning showed that adsorbed moisture increases the likelihood of flashing as compared to dry samples scanned at the same laser power and applied field. SEM observations of samples scanned at laser powers of 8-10 W and that

exhibited stage I SLFS showed that the resulting microstructures were similar for samples that were dry and those that were exposed to laboratory air prior to laser scanning (Figs. 12a and 12b). Similarly, for samples that exhibited stage II SLFS, there were no discernable differences in the microstructures for samples that were dry and those that were exposed to laboratory air prior to laser scanning (Figs. 12c and 12d).

Experiments conducted at higher laser powers of 20 W (Fig. 13) showed there is a strong effect of applied electric field on sintering. SEM observations of samples where no electric field was applied during laser scanning exhibited moderate coarsening and significant neck formation, but minimal densification compared to the original powder pellet. In contrast, samples where an electric field was applied during laser scanning exhibited nearly complete densification. These results show that electric field strongly influences SLFS. However, moisture did not significantly affect the microstructures for samples scanned at laser powers of 20 W. For example, there are no significant differences between the dry sample and the sample exposed to moistures for either samples scanned without a field or those scanned with an applied field of 3000 V/cm.

It is interesting that experiments showed that higher laser powers did not result in an increase in electrical current flow in the samples, and in fact the current actually decreased. This result is not intuitive since temperature and therefore conductivity increases with additional laser power. In many cases, we observed cracks in the laser path following laser scanning. The cracking was likely due to a combination of thermal shock and rapid shrinkage due to densification and thus cracking is more severe with increasing laser power. The cracks interrupt the conduction path and decrease the sample conductivity.

Our results suggest that the increase in conductivity that accompanies moisture adsorption facilitates the initiation of SLFS. However, once SLFS is initiated, the effects of moisture are fleeting. Joule heating that accompanies current flow leads to evaporation of the moisture. Thus, shortly after the initiation of SLFS, the conductivity of the powder pellet is likely similar whether the pellet started at out dry or was exposed to laboratory air. Since the observable changes to the microstructure such as coarsening and densification processes occur at higher temperatures than the temperature at which moisture evaporates, the presence or absence of moisture in the starting pellet does not strongly influence the final microstructure.

Conclusions

The effects of adsorbed moisture on SLFS of 8-YSZ was investigated by studying dry pellets and pellets that were in equilibrium with laboratory air. The laser scan speed was held constant at 100 mm/s while the laser power during scanning was varied between 8 - 20 W and the field strength was varied between 0 - 3000 V/cm. The current flowing through the sample was measured during the SLFS experiment and the microstructures were observed following SLFS in an SEM.

The results showed that SLFS is more easily initiated in samples containing adsorbed water as compared with dry samples. However, the moisture effects on SLFS decrease if the specimen is held in the SLFS machine prior to laser scanning because the samples dry as they are exposed to the nitrogen environment and the Joule heating that occurs from the applied electric field. SEM observations following SLFS did not reveal significant effects of moisture on the

final microstructures of samples that exhibited stage I or stage II SLFS. This is likely because moisture that is absorbed on the powder surfaces is removed at temperatures lower than that required for microstructural changes.

There are several challenges that remain before SLFS can be used as an additive manufacturing process. We have demonstrated that single layers specimens can be rapidly densified under the combination of an applied electric field and a scanning laser. To enable additive manufacturing using this process, it would need to be adapted to allow multi-layer SLFS to build up three dimensional parts. Equally importantly, a means for controlling local temperature at the temporal and spatial scales required to control the process is needed. This requires an accurate measurement of peak temperatures, time at temperature, and a means for controlling current flowing through the specimen.

Acknowledgements

We gratefully acknowledge support from the Office of Naval Research under the direction of Dr. Antti Makinen (grant number N00014-18-1-2261). Our deep appreciation extends to Mark Phillips for excellent engineering advice related to the equipment design and improvement of the selective laser flash sintering system and to Tim Phillips for aiding in temperature data analysis. We also acknowledge the assistance of Daniel Smith, Jamie Svrcek, Vickie Grier and John Lange.

References

1. J. Deckers, J. Vleugels, and J. P. Kruthl, "Additive Manufacturing of Ceramics: A Review," *J Ceram Sci Technol,* 5[4] 245-60 (2014).
2. A. Zocca, P. Colombo, C. M. Gomes, and J. Gunster, "Additive Manufacturing of Ceramics: Issues, Potentialities, and Opportunities," *Journal of the American Ceramic Society,* 98[7] 1983-2001 (2015).
3. U. Scheithauer, E. Schwarzer, H.-J. Richter, and T. Moritz, "Thermoplastic 3D Printing—An Additive Manufacturing Method for Producing Dense Ceramics," *International Journal of Applied Ceramic Technology,* 12[1] 26-31 (2015).
4. J. A. Lewis, J. E. Smay, J. Stuecker, and J. Cesarano, "Direct ink writing of three-dimensional ceramic structures," *Journal of the American Ceramic Society,* 89[12] 3599-609 (2006).
5. J. Deckers, S. Meyers, J. P. Kruth, and J. Vleugels, "Direct selective laser sintering/melting of high density alumina powder layers at elevated temperatures," *Physcs Proc,* 56 117-24 (2014).
6. M. Cologna, A. L. G. Prette, and R. Raj, "Flash-Sintering of Cubic Yttria-Stabilized Zirconia at 750 degrees C for Possible Use in SOFC Manufacturing," *Journal of the American Ceramic Society,* 94[2] 316-19 (2011).
7. M. Cologna, B. Rashkova, and R. Raj, "Flash Sintering of Nanograin Zirconia in < 5 s at 850 degrees C," *Journal of the American Ceramic Society,* 93[11] 3556-59 (2010).
8. R. Raj, "Joule heating during flash-sintering," *Journal of the European Ceramic Society,* 32[10] 2293-301 (2012).

9. J. S. C. Francis and R. Raj, "Influence of the Field and the Current Limit on Flash Sintering at Isothermal Furnace Temperatures," *Journal of the American Ceramic Society,* 96[9] 2754-58 (2013).
10. K. T. Shikhar K. JHA, Jean-Marie LEBRUN and Rishi RAJ, "Beyond flash sintering in 3 mol % yttria stabilized zirconia," *Journal of the Ceramic Society of Japan,* 124[4] P4-1-P4-4 (2016).
11. B. Dargatz, J. Gonzalez-Julian, M. Bram, Y. Shinoda, F. Wakai, and O. Guillon, "FAST/SPS sintering of nanocrystalline zinc oxide-Part II: Abnormal grain growth, texture and grain anisotropy," *Journal of the European Ceramic Society,* 36[5] 1221-32 (2016).
12. J. Y. Nie, Y. Y. Zhang, J. M. Chan, R. X. Huang, and J. Luo, "Water-assisted flash sintering: Flashing ZnO at room temperature to achieve similar to 98% density in seconds," *Scripta Materialia,* 142 79-82 (2018).
13. Deborah Hagen, Desiderio Kovar, Joseph J Beaman, "Selective laser flash sintering of 8-YSZ," *Journal of the American Ceramic Society* (2019).
14. Deborah Hagen, Joseph J. Beaman, Desiderio Kovar, "Effects of Electric Field on Selective Laser Sintering of Yttria-Stabilized Zirconia Ceramic Powder,″ pp. 909-13 in Solid Freeform Fabrication Symposium – An Additive Manufacturing Conference. (2018).
15. L. A. Dombrovsky, B. Rousseau, P. Echegut, J. H. Randrianalisoa, and D. Baillis, "High Temperature Infrared Properties of YSZ Electrolyte Ceramics for SOFCs: Experimental Determination and Theoretical Modeling," *Journal of the American Ceramic Society,* 94[12] 4310-16 (2011).